

# Spatial Brain Tumor Concentration Estimation for Individualized Radiotherapy Planning

Jonas Weidner<sup>1,2</sup>, Michal Balcerak<sup>3</sup>, Ivan Ezhov<sup>1,2</sup>, André Datchev<sup>1</sup>, Laurin Lux<sup>1,2</sup>, Lucas Zimmer<sup>1,2</sup>, Daniel Rueckert<sup>1,2,4</sup>, Björn Menze<sup>3</sup>, and Benedikt Wiestler<sup>1,2</sup>

<sup>1</sup> Technical University of Munich

<sup>2</sup> Munich Center for Machine Learning

<sup>3</sup> University of Zurich

<sup>4</sup> Imperial College London

j.weidner@tum.de

**Abstract.** Biophysical modeling of brain tumors has emerged as a promising strategy for personalizing radiotherapy planning by estimating the otherwise hidden distribution of tumor cells within the brain. However, many existing state-of-the-art methods are computationally intensive, limiting their widespread translation into clinical practice. In this work, we propose an efficient and direct method that utilizes soft physical constraints to estimate the tumor cell concentration from preoperative MRI of brain tumor patients. Our approach optimizes a 3D tumor concentration field by simultaneously minimizing the difference between the observed MRI and a physically informed loss function. Compared to existing state-of-the-art techniques, our method significantly improves predicting tumor recurrence on two public datasets with a total of 192 patients while maintaining a clinically viable runtime of under one minute - a substantial reduction from the 30 minutes required by the current best approach. Furthermore, we showcase the generalizability of our framework by incorporating additional imaging information and physical constraints, highlighting its potential to translate to various medical diffusion phenomena with imperfect data.

**Keywords:** Brain Tumor · Radiotherapy · Biophysical Modeling · Partial Differential Equation

## 1 Introduction

The treatment of glioblastoma, the most aggressive primary brain tumor, presents a severe clinical challenge with persistently low survival rates. A key reason for this is the diffuse spread of tumor cells into the surrounding brain, which are the main targets for postoperative radiotherapy. However, this spread is mostly invisible in standard magnetic resonance imaging (MRI), and current radiotherapy treatment planning relies on a simple protocol [12]: a uniform 15mm margin is drawn around the resection cavity to account for microscopic tumor cell infiltration.

Tumor growth modeling promises to reveal the otherwise invisible tumor cell infiltration, enabling truly personalized radiotherapy and improving patient outcomes. Diverse approaches have been developed in this direction. Traditionally, pure bio-physical models were fitted with compute-intensive sampling approaches [11]. Learning-based approaches [7] have shown dramatic speedups but often lack precision. Combining both approaches by using deep learning estimation as a prior for subsequent sampling reduces runtime and enhances precision but still falls short of the runtime achieved by purely deep learning-based methods [16]. Path-based methods like [4] provide a simple geometric evolution but lack evaluation on recurrence prediction in a patient cohort.

Recent sophisticated approaches [2,3] demonstrate that advanced models, incorporating brain deformation, several imaging modalities, and physical tumor properties, can precisely capture the tumor growth process while outperforming conventional methods in tumor recurrence prediction. These methods fit a discrete 4D (3D plus time) tumor cell concentration to the data while preserving a physically plausible growth process. With modern optimization frameworks, this process can be calculated within about one hour on modern GPUs. However, many assumptions are required, as well as heuristics, for fine-tuning. For clinical practice, a faster calculation time would be highly beneficial.

In response to these challenges, we propose a streamlined method for estimating tumor concentration. Rather than modeling the entire growth process, our approach optimizes the tumor concentration to adhere to a locally plausible shape while explaining the measured data solely within the spatial 3D domain, as typically only a single time point—when the tumor has already grown—is accessible. To facilitate this, we develop differentiable loss terms that can be efficiently optimized using modern machine learning frameworks, integrating both data and physics loss components. Although our method does not encompass the full simulation process, we demonstrate state-of-the-art performance in predicting tumor recurrence across two public datasets, outperforming existing methods with a runtime of under one minute. Our main contributions are:

1. We introduce a *combined physics and data loss formulation* to fit the tumor concentration to the data while simultaneously adhering to physical constraints.
2. We demonstrate that our method *improves radiotherapy planning and recurrence prediction* over state-of-the-art methods at a fraction of the time.
3. We showcase the *extensibility and adaptability* of our method by including different imaging modalities like PET and additional physical constraints.

## 2 Methods

We propose a new way of estimating how tumor cells spread in the brain. The tumor concentration describes the proportion of tumor cells in every voxel of the brain. We want to fit this tumor concentration for each voxel to the data while simultaneously following a physically plausible distribution. Therefore, we

optimize the tumor cell concentration in each voxel based on the gradients of the differentiable loss terms. Based on the proposed tumor concentration, we construct a radiotherapy plan, which we evaluate in terms of its ability to predict tumor recurrence against the clinical state-of-the-art and several competing computational methods. An overview of our method is given in Figure 1.

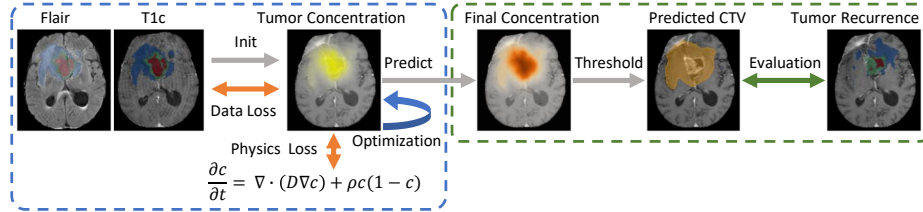


**Fig. 1.** We optimize (blue) a 3D scalar tumor concentration estimation (yellow) by simultaneously fitting the data and regularizing on physical properties. Using this predicted tumor concentration (orange), we propose a radiotherapy plan (Clinical Target Volume (CTV), orange). We evaluate (green) our method’s ability to capture areas with later tumor recurrence.

## 2.1 Loss

We optimize the tumor concentration in each voxel, minimizing a differentiable loss function. Our framework combines two distinct losses: data and physics loss  $L$  with weights  $\lambda$ . While the *data loss* closely matches the predicted tumor cell concentration to the visible tumor in the MRI, the *physics loss* ensures that the proposed final tumor concentration follows a physically plausible distribution:

$$L_{\text{Total}} = \lambda_{\text{Data}} L_{\text{Data}} + \lambda_{\text{Physics}} L_{\text{Physics}} \quad (1)$$

**Data Loss** We use MR images to compute a data loss. We use contrast-enhanced T1c and Flair images to segment the tumor in enhancing tumor and necrotic areas (combined into  $S_{\text{Core}}$ ), and edema ( $S_{\text{Edema}}$ ) using BRATS toolkit [8]. As low tumor concentrations are not visible in MR images, we introduce certain thresholds for the tumor core  $\tau_{\text{Core}}$  and edema  $\tau_{\text{Edema}}$  above which the tumor is assumed to be visible. For the data loss, we use the Dice score ( $DSC$ ) [6] between the predicted tumor concentration above the threshold and the segmentation derived from the MRI:

$$L_{\text{Data}} = \alpha_{\text{Core}} DSC(\hat{c} > \tau_{\text{Core}}, S_{\text{Core}}) + \alpha_{\text{Edema}} DSC(\hat{c} > \tau_{\text{Edema}}, S_{\text{Edema}}) \quad (2)$$

Opposed to directly using the Dice loss on the estimated tumor concentration  $\hat{c}$ , we threshold the concentration according to the predefined thresholds for tumor core ( $\tau_{\text{Core}}$ ) and edema  $\tau_{\text{Edema}}$ . This circumvents the problem of forcing all concentrations above the thresholds to 1, which is physically unrealistic. Our formulation does not penalize concentrations on the correct side of the threshold. This allows a soft fade-out of the concentrations at the segmentation edge, which matches the typical infiltration gradient these tumors show.

**Physics Loss** The growth of a tumor is typically modeled by a reaction-diffusion partial differential equation (PDE), like the Fisher-Kolmogorov equation:

$$\frac{\partial c}{\partial t} = \nabla \cdot (D \nabla c) + \rho c(1 - c) \quad (3)$$

The temporal development of the tumor concentration  $c$  is described by the logistic growth parameter  $\rho$  and the diffusion coefficient  $D$ . In literature, many variations of this equation exist using different growth terms, different tumor diffusion coefficients for other tissue types, and additional terms like advection [14,13].

For our framework, we exploit a common pattern of these PDE models: Reaction-diffusion equations naturally yield solutions that are well-behaved in both space and time, characterized by continuous changes and the absence of abrupt variations. The diffusion term plays a key role by spreading out localized differences, ensuring a gradual transition across spatial regions. Similarly, the reaction term, typically defined as smooth functions of the state variables, maintains this regularity without introducing discontinuities. Even if sharp features arise from initial or boundary conditions, the diffusion process quickly moderates them. Therefore, we limit the change in tumor concentration in neighboring voxels as the  $L_2$ -loss of the gradient magnitude normalized by the number of voxels  $N$ .

$$L_{\text{Physics}} = \frac{1}{N} \sum_{n=1}^N |\nabla \hat{c}_n|^2 \quad (4)$$

## 2.2 Evaluation

To evaluate the estimated tumor concentration, we test its ability to predict tumor recurrence. We assume that post-operative tumor recurrence is correlated with preoperative tumor cell concentration. Importantly, this metric also directly links our method with informing individualized radiotherapy plans based on estimated tumor cell concentrations.

**Metric** We create synthetic standard plans following the current clinical guidelines [12] in the same way as done by [3]. We use the volume of the tumor core as an approximation for the resection cavity and an additional, isotropic 15 mm

margin around it inside the brain. This total volume serves as a reference volume for other methods. We construct a proposed CTV with the same volume as the standard plan for each compared method. Then, we measure the percentage of tumor recurrence covered by this binarized volume. For a more nuanced evaluation, we distinguish between the prediction of "enhancing recurrence" and "any recurrence", which is the area of edema, necrotic, or enhancing recurrence.

**Statistical evaluation** We always compare paired data for different methods. Additionally, the results are typically not normally distributed, as the recurrence is often covered completely by all methods or not covered at all, validated by the Shapiro-Wilk test. Thus, we used the paired Wilcoxon-ranked test if not stated otherwise. We marked significant results with "\*" for  $p < 0.05$  and "\*\*" for  $p < 0.01$ . For comparison to the next best baseline method, "static grid discretization", we use "†" and "‡". The reported standard errors in the table are based on the standard deviation within the whole patient cohort. So, they are meant to measure the deviation between the patients instead of determining the difference in method performance.

**Datasets** For our experiments, we require both the preoperative MRI (to estimate tumor cell concentrations) as well as a later follow-up MRI showing tumor recurrence, which needs to be registered to the preoperative space to allow for evaluation. We use the following two public datasets:

- **GliODIL** contains 152 glioblastoma patients [3], with estimated tissue concentrations and segmentations of tumor and tumor recurrence (warped to the preop space). Additionally, FET-PET imaging is available for a subset of 58 patients.
- **RHUH** contains pre-operative, post-operative, and recurrence MR images of 40 patients and segmentations. We employed ANTs with the optimized settings from the BraTSReg challenge [1] to deformably register recurrence into preop space. It is used to demonstrate the generalizability of our method to different scanners and populations [5].

### 2.3 Baseline Methods

We compare our method to the clinical standard treatment plan and other state-of-the-art methods.

- **Standard Plan** refers to the standard procedure defining the recurrence prediction volume for all other methods. A 15 mm margin is constructed around the enhancing recurrence.
- **Numerical Physics Simulations**, which utilizes the evolutionary sampling strategy of numerically simulated tumors [16].
- **Data-Driven Neural Networks (Unconstrained)** describes the UNet adaptation introduced by [3].

- **Data-Driven Neural Networks (Physics-Constrained)** refers to the neural inverse solver by [7].
- **Static Grid Discretization** optimizes the 3D + time tumor growth process on a static grid constrained by physically plausible timesteps [3].
- **Deformable Grid Discretization** extends the Static Grid Discretization by a deformable mesh and PET image information [2].

## 2.4 Extending our framework

Besides its primary contribution, the combined data & physics loss function, our framework is designed to be expandable through additional loss terms that add specific objectives or constraints. Here, we demonstrate how (i) advanced imaging modalities can be included as additional data loss and (ii) further physical constraints may be utilized to improve the physics loss.

**Including Additional Imaging Modalities** In brain tumors, several imaging modalities are used. Besides the most common MR sequences, Flair and T1c, from which we extract the edema and core segmentations, several other imaging modalities are typically acquired. These modalities contain relevant information for understanding the tumor dynamics. In this example, we focus on positron emission tomography (PET) imaging. It was shown that PET image intensity  $I_{\text{PET}}$  correlates with tumor concentration inside the edema region [10]. To incorporate this into our estimation of tumor cell concentration, we define a new loss term as:

$$L_{\text{PET}} = \text{corr}(\hat{c}, I_{\text{PET}}) \quad (5)$$

Resulting in the new total loss:

$$L_{\text{Total+PET}} = \lambda_{\text{Data}}L_{\text{Data}} + \lambda_{\text{Physics}}L_{\text{Physics}} + \lambda_{\text{PET}}L_{\text{PET}} \quad (6)$$

**Including Further Physical Constraints** It can be shown that a traveling wave in the form of a sigmoid solves equation 3 in one dimension [15]. After a tumor grows to a large size, compared to the origin cell concentration, the exact initial condition becomes unimportant [9]:

$$c(x, t) = \left( 1 + \exp \left( \frac{x - 2\sqrt{D\rho t}}{\sqrt{\frac{D}{\rho}}} \right) \right)^{-1} \quad (7)$$

$$\frac{\partial c}{\partial x} = \sqrt{\frac{\rho}{D}}c(1 - c) \quad (8)$$

We assume this sigmoid behavior locally at a given time. Thus, we can conclude that the following condition must be fulfilled for the predicted tumor concentration  $\hat{c}$ :

$$|\nabla \hat{c}| \stackrel{!}{=} \left| \frac{\partial c}{\partial x} \right| \quad (9)$$

If we plug in the analytical solution (equation 8) we get the following:

$$|\nabla \hat{c}| = \left| \sqrt{\frac{\rho}{D}} \hat{c}(1 - \hat{c}) \right| \quad (10)$$

$\rho$  and  $D$  depend on the brain tissue and can be summarized with the function  $f$ . We can approximate  $f$  as a constant  $k$  for the assumption of isotropic and homogeneous brain anatomy. The constant  $k$  can be interpreted as the slope coefficient of the tumor, describing the steepness of the tumor concentration wavefront.

$$f(x) = \sqrt{\frac{\rho}{D(x)}} \approx k \quad (11)$$

The loss over all  $N$  voxels is defined as the mean squared error of the residuals of eq. 10, normalized by  $k$ :

$$L_{\text{Wave}} = \frac{1}{N} \sum_{n=1}^N \left( \frac{1}{k} (|\nabla \hat{c}_n| - k \hat{c}_n(1 - \hat{c}_n)) \right)^2 \quad (12)$$

This normalization is done to prevent the simple solution of a homogeneous tumor concentration. The final loss can now be described as:

$$L_{\text{Total+Wave}} = \lambda_{\text{Physics}} L_{\text{Physics}} + \lambda_{\text{Data}} L_{\text{Data}} + \lambda_{\text{Wave}} L_{\text{Wave}} \quad (13)$$

## 2.5 Optimization

The tumor concentration in each voxel is optimized after initializing it based on the thresholds of the tumor core and edema, ensuring minimal data loss. The initial concentrations are set as  $c_{i_{\text{Core}}} = \tau_{\text{Core}} + 0.01$ ,  $c_{i_{\text{Edema}}} = \tau_{\text{Edema}} + 0.01$ ,  $c_{i_{\text{Brain}}} = 0.01$  for the rest of the brain. The slope for the wave loss was initialized as  $k_{i_{\text{Wave}}} = 0.1 \text{ mm}^{-1}$ . The loss weights were selected so that the losses were of a similar order of magnitude:  $\alpha_{\text{Core}} = 1$ ,  $\alpha_{\text{Edema}} = 1$ ,  $\lambda_{\text{Data}} = 1$ ,  $\lambda_{\text{Physics}} = 10 \text{ cm}^2$ ,  $\lambda_{\text{Wave}} = 1000$ , and  $\lambda_{\text{PET}} = 1$ . We sampled the thresholds  $\tau_{\text{Core}}$  from 0.6, 0.7, 0.8, 0.9 and  $\tau_{\text{Edema}}$  from 0.1, 0.2, 0.3, 0.4, 0.5. The optimization process run for 500 steps.

As it is hard to define clear thresholds  $\tau_{\text{Core}}$  and  $\tau_{\text{Edema}}$  for the visible tumor concentration, we decided to test a wide range of clinically plausible choices. In our approach, these thresholds not only represent the visible tumor concentration, but regarding the recurrence prediction, their ratio is crucial for weighting edema and tumor core. Despite numerical instabilities in some experiments, this dual meaning is the reason why we did not optimize the tumor thresholds. For optimization, we utilize the highly optimized PyTorch GPU implementation of the Adam optimizer. We published our code at "<https://github.com/jonasw247/spatial-brain-tumor-concentration-estimation>".

### 3 Results

We evaluate our results mainly on the GliODIL dataset with 152 patients. We measure the recurrence coverage, that is, the ratio of tumor recurrence, which is covered by the proposed radiation plan. A qualitative assessment of how our method compares against the current standard procedure is shown in Figure 2. The visual assessment highlights the crucial role of the edema region. Although it is ignored in the standard procedure, there is a clear indication that edema has a predictive correlation with tumor recurrence. We find this is also the largest benefit over the best baseline method, "static grid discretization".

The quantitative results of our method are shown in Table 1. We compare our data to the state-of-the-art models in our field, [3,7,16]. We see that our method outperforms all existing methods in predicting any recurrence, meaning edema, necrosis, or enhancing core, and also in predicting only contrast-enhancing tumor recurrence, while only the worst thresholds lead to significant results, which occurs due to the applied non-parametric rank test.

**Table 1.** Comparison of recurrence segmentation coverage given equal radiation volume, tested for different edema and core thresholds (Figure 3). Our method outperforms all others with short runtime.

Recurrence Coverage - GliODIL (152 Patients)	Any [%]	Enhancing Core [%]	Runtime
NN (Unconstrained)	65.38 $\pm$ 2.05	69.02 $\pm$ 2.79	< 1 min
NN (Physics-Constrained)	62.06 $\pm$ 2.11	75.25 $\pm$ 2.84	< 1 min
Numerical Physics Simulations	61.16 $\pm$ 2.12	75.34 $\pm$ 2.87	2 h
Static Grid Discretization	67.80 $\pm$ 2.09	84.42 $\pm$ 2.40	30 min
Standard Plan	63.59 $\pm$ 2.26	82.42 $\pm$ 2.60	< 1 min
Ours Worst Thresholds	69.72 $\pm$ 2.07 <sup>†**</sup>	84.34 $\pm$ 2.38 <sup>**</sup>	1 min
Ours Median Thresholds	70.93 $\pm$ 1.99 <sup>†**</sup>	85.02 $\pm$ 2.31	1 min
Ours Best Thresholds	<b>72.48 <math>\pm</math> 1.99<sup>†**</sup></b>	<b>85.19 <math>\pm</math> 2.28</b>	1 min

As it is unclear which tumor concentrations are visible in MR images, we tested an extensive, medically plausible range of thresholds  $\tau_{\text{Core}}$  and  $\tau_{\text{Edema}}$ . For our comparison on recurrence prediction, these tumor thresholds can also be interpreted as the weighting between the importance of tumor core *vs.* edema. We show the sweep over those thresholds in Figure 3.

In general, we do not find a large variation for different thresholds. Predicting the enhancing recurrence is slightly easier when selecting a high core threshold. For the "any recurrence" prediction, we find an optimal outcome at ( $\tau_{\text{Core}} = 0.6$ ,  $\tau_{\text{Edema}} = 0.2$ ). We assume this relatively even distribution of the tumor concentration range between 0 and 1 leaves a good distance between two thresholds, holding an optimal range that fits the physics loss.

#### 3.1 Replication Study on RHUH Dataset

To validate our findings, we compare our method with the standard plan and the best baseline method on the independent RHUH dataset, which stems from



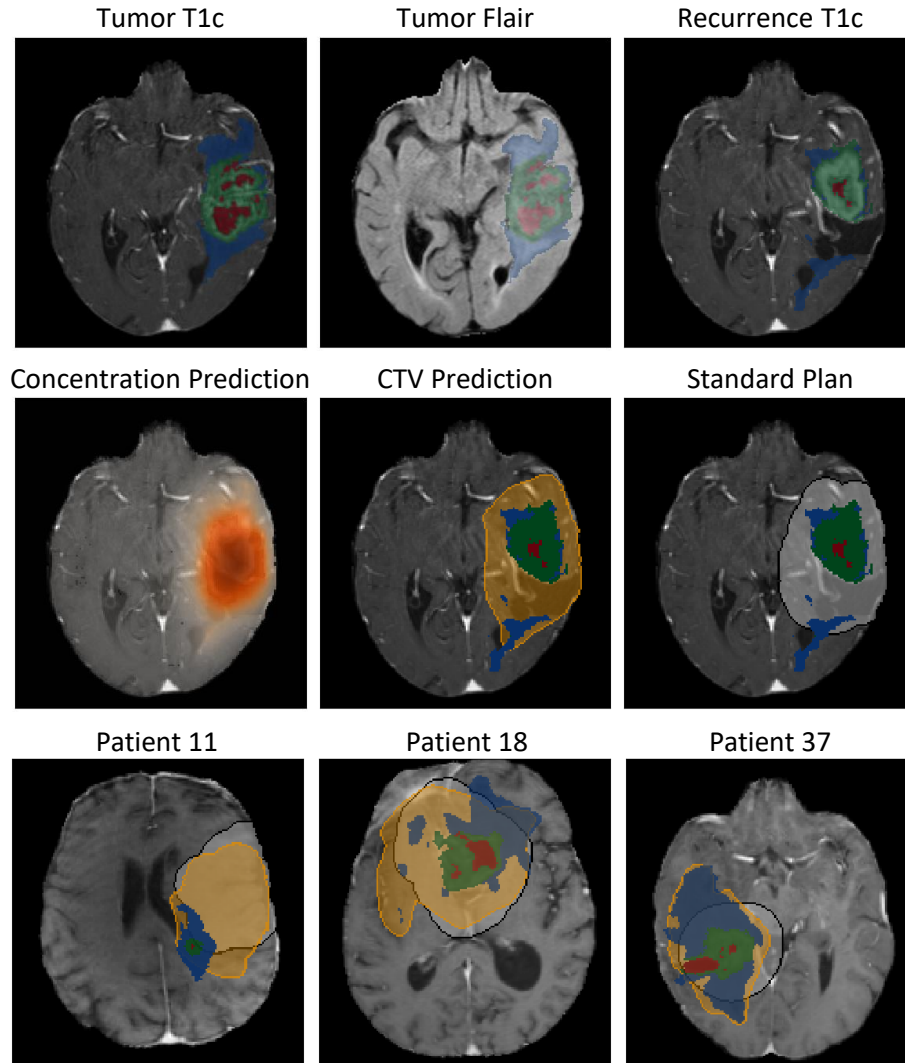


**Fig. 2.** Demonstration of our method on example patients. In the first row, we show the two input MR images with the tumor and the recurrence, that should be covered. Edema is shown in blue, enhancing tumor in green, and necrotic in red. Our method predicts a continuous assumption of tumor cells shown in the second row. This continuous concentration is thresholded to have the same volume as the standard plan (grey) to create the CTV (orange). In the last row, we compare our method to the standard plan for different patients. the same result for additional patients from the RHUH dataset.

another center. The results are shown in Table 2. We find similar results to those on the primary dataset. For "any recurrence," we see a significant improvement

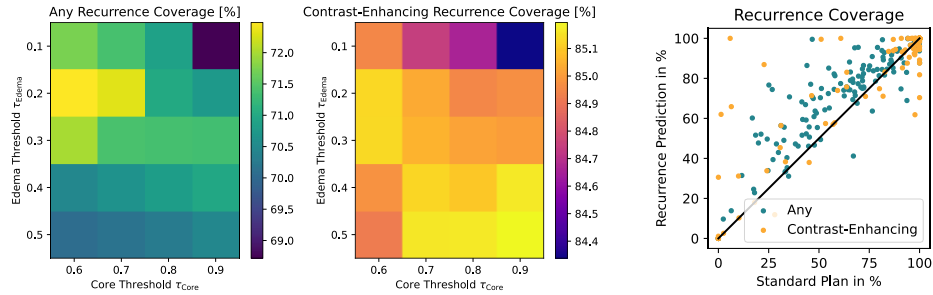


**Fig. 3.** The recurrence coverage is shown for the GliODIL Dataset with 152 patients comparing contrast-enhancing recurrence (orange) and any recurrence (green). Different core and edema visibility threshold parameters  $\tau$  are tested. On the right, the individual results for each patient are shown compared to the standard plan. A clear improvement is visible for many patients, while also a lot of patients result in 0% or 100% coverage.

of 5% to 8% compared to the standard plan. Identical to the GliODIL dataset, the improvement in predicting the contrast-enhancing part of the results is about 2% to 3%.

**Table 2.** We evaluated our method on the independent second RHUH Dataset with 40 patients. We compared our method to the standard plan and the best-performing baseline from the GliODIL dataset.

Recurrence Coverage - RHUH (40 Patients)	Any [%]	Enhancing Core [%]
Static Grid Discretization	$70.95 \pm 3.29$	$85.36 \pm 5.4$
Standard Plan	$65.47 \pm 3.51$	$85.06 \pm 5.4$
Ours Worst	$70.27 \pm 3.28^{**}$	$86.91 \pm 4.93$
Ours Median	$72.02 \pm 3.21^{**}$	$87.15 \pm 5.03$
Ours Best	$73.18 \pm 3.16^{\dagger**}$	$87.48 \pm 4.90$

### 3.2 Extending Our Framework

We evaluate how our method can be extended. Therefore, we conduct two additional experiments, where we (i) include advanced imaging data and (ii) add a further physical loss into the tumor cell estimation.

**Including PET Imaging** As an example of how our method can be extended with additional measurements, we evaluate the effects of an additional PET loss. We tested 58 patients who had amino acid PET images in the GliODIL dataset. The same experiment was conducted by [2] in a recent NeurIPS publication, simulating not only the influence of PET but also advanced brain deformations.

In Table 3, we compare the default method with optimal parameters and our method with the additional PET loss to this method and to the other methods also used for the full GliODIL dataset (Table 1). Both the default method and the one including PET loss show a clear improvement over the standard plan and over the dynamic grid discretization in terms of "any recurrence" prediction. In enhancing recurrence coverage, the dynamic grid discretization is better than our method, while our methods are slightly still outperforming the standard plan. For this, the distribution is also highly dominated by outliers, as most patients already have 100% enhancing recurrence coverage in the standard plan.

**Table 3.** Comparison of our additional method utilizing PET imaging. We use the subset of 58 patients of the Gliod dataset having PET imaging. Additionally, we can compare our results to the method "Dynamic Grid Discretization"[2], which requires PET.

Recurrence Coverage with PET (58 Patients)	Any [%]	Enhancing Core [%]
NN (Unconstrained)	59.0 $\pm$ 4.3	66.8 $\pm$ 4.9
NN (Physics-Constrained)	70.4 $\pm$ 3.7	84.3 $\pm$ 3.3
Numerical Physics Simulations	67.1 $\pm$ 3.8	86.2 $\pm$ 3.6
Static Grid Discretization	72.9 $\pm$ 3.5	89.0 $\pm$ 3.3
Dynamic Grid Discretization	74.7 $\pm$ 3.1	<b>89.9 <math>\pm</math> 2.7</b>
Standard Plan	70.0 $\pm$ 3.8	87.3 $\pm$ 3.6
Ours	76.2 $\pm$ 3.4 <sup>†**</sup>	88.2 $\pm$ 3.4
Ours with additional PET Loss	<b>77.4 <math>\pm</math> 3.3<sup>†**</sup></b>	88.4 $\pm$ 3.3

**Including Further Physical Constraints** As an additional loss, we test how the assumption of a wave-like solution affects the recurrence prediction. We ran the same tumor visibility parameter sweep as shown in Figure 3 with the additional wave loss. The results are compared to the default loss and are shown in Table 4. We see a clear improvement for the median and the worst set of thresholds in predicting "any recurrence". Additionally, by using the wave loss, we get significant results for the prediction of the enhancing core. This can be interpreted as increased robustness towards the selection of hyperparameters, paving the way for further adjustment of advanced physics constraints and highlighting how extending our framework with additional physical constraints can improve model safety, an important prerequisite for clinical translation.

## 4 Discussion

In this study, we demonstrated that our approach, which efficiently combines soft physical constraints and direct optimization of 3D tumor concentration to imaging data, shows promising results for recurrence prediction while substantially reducing computational demand compared to other methods. With a runtime of

**Table 4.** Recurrence prediction with the additional assumption of a wave-like solution compared to the default version of our method. We compare the minimum, maximum, and median of recurrence coverage with multiple thresholds as shown in Figure 3.

Recurrence Coverage - with Wave Loss (152 Patients)	Any [%]	Enhancing Core [%]
Ours Worst Thresholds	69.72 $\pm$ 2.07 <sup>‡**</sup>	84.34 $\pm$ 2.38 <sup>**</sup>
Ours Median Thresholds	70.93 $\pm$ 1.99 <sup>‡**</sup>	85.02 $\pm$ 2.31
Ours Best Thresholds	<b>72.48</b> $\pm$ 1.99 <sup>‡**</sup>	85.19 $\pm$ 2.28
Ours with Wave Loss Worst Thresholds	71.24 $\pm$ 2.08 <sup>‡**</sup>	84.79 $\pm$ 2.34
Ours with Wave Loss Median Thresholds	71.79 $\pm$ 2.07 <sup>‡**</sup>	85.03 $\pm$ 2.35 <sup>‡*</sup>
Ours with Wave Loss Thresholds	72.16 $\pm$ 2.06 <sup>‡**</sup>	<b>85.46</b> $\pm$ 2.32 <sup>‡**</sup>

under one minute, our approach is markedly faster than the 30+ minutes typically required by current state-of-the-art methods. By eliminating the need for extensive simulations of tumor growth dynamics, our method facilitates practical integration into existing radiotherapy workflows, thereby enhancing the efficiency of patient-specific treatment planning.

#### 4.1 Limitations

It is relevant to acknowledge that our method does not capture the complete trajectory of tumor growth, which may limit its utility in understanding past tumor growth dynamics. While some extrapolation may be possible based on the optimized tumor concentration, our approach does not support retrospective modeling. Furthermore, the application of radiation was conducted solely based on standard planning methods, which could potentially influence recurrence rates in the treated region.

#### 4.2 Outlook

Importantly, our framework can easily be extended to incorporate advanced imaging methods as well as additional physical constraints. Our experimental results indicate that these enhancements, particularly the inclusion of extra physical constraints, can "stabilize" predictions and provide essential safety guarantees, which are critical for clinical translation and effective radiotherapy planning. Moreover, this versatility suggests that our framework could be applied to a broader range of medical challenges beyond brain tumor modeling, such as predicting the spread of infection.

## References

1. Baheti, B., Waldmannstetter, D., Chakrabarty, S., Akbari, H., Bilello, M., Wiestler, B., Schwarting, J., Calabrese, E., Rudie, J., Abidi, S., et al.: The brain tumor sequence registration challenge: establishing correspondence between pre-operative and follow-up mri scans of diffuse glioma patients. arXiv preprint arXiv:2112.06979 (2021)

2. Balcerak, M., Amiranashvili, T., Wagner, A., Weidner, J., Karnakov, P., Paetzold, J.C., Ezhov, I., Koumoutsakos, P., Wiestler, B., et al.: Physics-regularized multi-modal image assimilation for brain tumor localization. In: The Thirty-eighth Annual Conference on Neural Information Processing Systems
3. Balcerak, M., Ezhov, I., Karnakov, P., Litvinov, S., Koumoutsakos, P., Weidner, J., Zhang, R.Z., Lowengrub, J.S., Wiestler, B., Menze, B.: Individualizing glioma radiotherapy planning by optimization of a data and physics informed discrete loss. arXiv preprint arXiv:2312.05063 (2023)
4. Bortfeld, T., Buti, G.: Modeling the propagation of tumor fronts with shortest path and diffusion models—implications for the definition of the clinical target volume. *Physics in Medicine & Biology* **67**(15), 155014 (2022)
5. Cepeda, S., García-García, S., Arrese, I., Herrero, F., Escudero, T., Zamora, T., Sarabia, R.: The río hortega university hospital glioblastoma dataset: A comprehensive collection of preoperative, early postoperative and recurrence mri scans (rhuh-gbm). *Data in Brief* **50**, 109617 (2023)
6. Dice, L.R.: Measures of the amount of ecologic association between species. *Ecology* **26**(3), 297–302 (1945)
7. Ezhov, I., Scibilia, K., Franitza, K., Steinbauer, F., Shit, S., Zimmer, L., Lipkova, J., Kofler, F., Paetzold, J.C., Canalini, L., et al.: Learn-morph-infer: a new way of solving the inverse problem for brain tumor modeling. *Medical Image Analysis* **83**, 102672 (2023)
8. Kofler, F., Berger, C., Waldmannstetter, D., Lipkova, J., Ezhov, I., Tetteh, G., Kirschke, J., Zimmer, C., Wiestler, B., Menze, B.H.: Brats toolkit: translating brats brain tumor segmentation algorithms into clinical and scientific practice. *Frontiers in neuroscience* p. 125 (2020)
9. Konukoğlu, E., Clatz, O., Bondiau, P.Y., Delingette, H., Ayache, N.: Extrapolating tumor invasion margins for physiologically determined radiotherapy regions. In: *Medical Image Computing and Computer-Assisted Intervention—MICCAI 2006: 9th International Conference, Copenhagen, Denmark, October 1-6, 2006. Proceedings, Part I* 9. pp. 338–346. Springer (2006)
10. Liesche-Starnecker, F., Prokop, G., Yakushev, I., Preibisch, C., Delbridge, C., Meyer, H.S., Aftahy, K., Barz, M., Meyer, B., Zimmer, C., et al.: Visualizing cellularity and angiogenesis in newly-diagnosed glioblastoma with diffusion and perfusion mri and fet-pet imaging. *EJNMMI research* **11**, 1–6 (2021)
11. Lipkova, J., Angelikopoulos, P., Wu, S., Alberts, E., Wiestler, B., Diehl, C., Preibisch, C., Pyka, T., Combs, S.E., Hadjidoúkas, P., et al.: Personalized radiotherapy design for glioblastoma: integrating mathematical tumor models, multi-modal scans, and bayesian inference. *IEEE transactions on medical imaging* **38**(8), 1875–1884 (2019)
12. Niyazi, M., Andratschke, N., Bendszus, M., Chalmers, A.J., Erridge, S.C., Galldiks, N., Lagerwaard, F.J., Navarria, P., af Rosenschöld, P.M., Ricardi, U., et al.: Estroeano guideline on target delineation and radiotherapy details for glioblastoma. *Radiotherapy and Oncology* **184**, 109663 (2023)
13. Saut, O., Lagaert, J.B., Colin, T., Fathallah-Shaykh, H.M.: A multilayer grow-or-go model for gbm: effects of invasive cells and anti-angiogenesis on growth. *Bulletin of mathematical biology* **76**, 2306–2333 (2014)
14. Subramanian, S., Gholami, A., Biros, G.: Simulation of glioblastoma growth using a 3d multispecies tumor model with mass effect. *Journal of mathematical biology* **79**, 941–967 (2019)

15. Swanson, K.R., Rostomily, R.C., Alvord, E.: A mathematical modelling tool for predicting survival of individual patients following resection of glioblastoma: a proof of principle. *British journal of cancer* **98**(1), 113–119 (2008)
16. Weidner, J., Ezhov, I., Balcerak, M., Metz, M.C., Litvinov, S., Kaltenbach, S., Feiner, L., Lux, L., Kofler, F., Lipkova, J., et al.: A learnable prior improves inverse tumor growth modeling. *IEEE Transactions on Medical Imaging* **PP** (Nov 2024). <https://doi.org/10.1109/TMI.2024.3494022>, <https://doi.org/10.1109/TMI.2024.3494022>